Fast Assembly of Ordered Block Copolymer Nanostructures through Microwave Annealing

Xiaojiang Zhang,[†,‡] Kenneth D. Harris,[†,*] Nathanael L. Y. Wu,[†,§] Jeffrey N. Murphy,[†,‡] and Jillian M. Buriak[†,‡,*]

[†]National Institute for Nanotechnology, National Research Council, 11421 Saskatchewan Drive, Edmonton, Alberta T6G 2M9, Canada, [‡]Department of Chemistry, University of Alberta, Edmonton, Alberta T6G 2G2, Canada, and [§]Department of Electrical and Computer Engineering, University of Alberta, Edmonton, Alberta T6G 2G8, Canada

ABSTRACT Block copolymer self-assembly is an innovative technology capable of patterning technologically relevant substrates with nanoscale precision for a range of applications from integrated circuit fabrication to tissue interfacing, for example. In this article, we demonstrate a microwave-based method of rapidly inducing order in block copolymer structures. The technique involves the usage of a commercial microwave reactor to anneal block copolymer films in the presence of appropriate solvents, and we explore the effect of various parameters over the polymer assembly speed and defect density. The approach is applied to the commonly used poly(styrene)-*b*-poly(methyl methacrylate) (PS-*b*-PMMA) and poly(styrene)-*b*-poly(2-vinylpyridine) (PS-*b*-P2VP) families of block copolymers, and it is found that the substrate resistivity, solvent environment, and anneal temperature all critically influence the self-assembly process. For selected systems, highly ordered patterns were achieved in less than 3 min. In addition, we establish the compatibility of the technique with directed assembly by graphoepitaxy.

KEYWORDS: block copolymer · solvothermal annealing · self-assembly · patterning · microwaves · platinum nanostructures · silicon substrate · graphoepitaxy

As photolithographic technologies are continuously refined and optimized, ever-improving pattern resolutions and feature densities are achieved on-chip. This technology underpins the entire integrated circuits industry, and yet it is ultimately expected to reach fundamental resolution limits.[1−3] As a result, new strategies are being sought to complement photolithography and achieve next generation requirements in a cost-effective manner. Among the array of possibilities, self-assembly is emerging as a powerful option, and the use of self-assembled block copolymers (BCPs) to generate organized nanostructures is becoming the subject of intense research.[4−12] Recent editions of the Semiconductor Industry Association's International Technology Roadmap for Semiconductors (ITRS), in fact, explicitly include templating with BCPs as an emerging technology for generating high-resolution patterns.[13] With these soft polymeric materials, the size and spacing of structures can be tuned by selecting appropriate polymer block lengths,[4] and nanostructures as small as 3 nm in diameter can be generated.[14] Organized patterns that reliably persist across long distances have been achieved, and in many cases, this is done while maintaining low defect densities.[14−18]

One design issue less frequently addressed is the BCP assembly speed.[19] The ITRS 2007 edition stipulates that "the net time required to form and fix a pattern must be short, less than four minutes",[20] and yet in most conventional BCP organization processes, a prolonged annealing step is reported. The anneal is intended to increase mobility of the polymer by directly elevating the temperature (*i.e.*, a thermal anneal) or plasticizing the network through extensive solvation of the polymer blocks (*i.e.*, a solvent anneal). These anneals allow the BCP to attain a thermodynamic minimum with respect to its organization. Beautiful work has shown that on prepatterned, functionalized surfaces with features matching the bulk lamellar period (L_0) of the BCPs (~48 nm, produced *via* extreme ultraviolet lithography), short annealing times (1 min) are effective,[21] but on flat, unpatterned surfaces, the lengthy processing times (hours to days)[4,22] for linear patterns may limit commercialization opportunities. Since one important aspect of BCP lithography is the harnessing of the natural nanoscale phase segregation of the polymers to produce organic nanopatterned templates on featureless regions of a surface, a route toward rapid anneals is critical. In this paper, we demonstrate a high-speed microwave annealing approach in which solvent-driven and thermally driven mechanisms act in concert to generate highly organized BCP patterns in minutes. The use of microwaves

*Address correspondence to jburiak@ualberta.ca, ken.harris@nrc.ca.

Received for review September 13, 2010 and accepted October 12, 2010.

Published online October 21, 2010. 10.1021/nn102387c

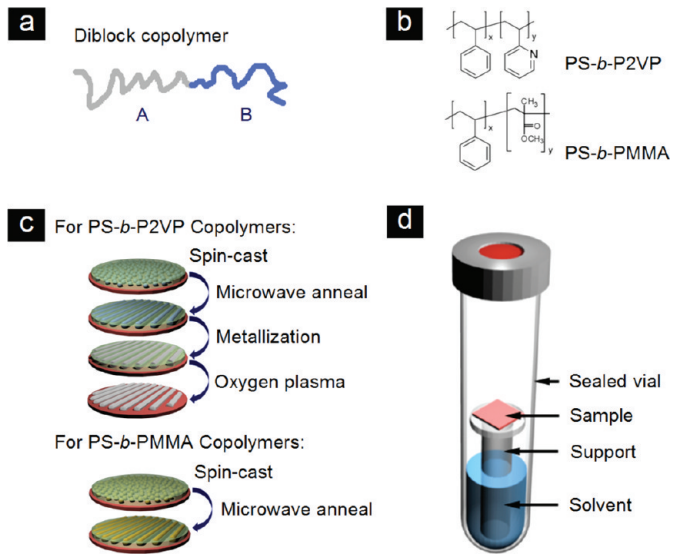

Figure 1. Schematic representation of the microwave annealing process. (a) Generalized structure of an AB diblock copolymer, and (b) chemical structures of the PS-*b*-P2VP and PS-*b*-PMMA block copolymers used in this study. (c) Schematic of experimental approach: a BCP film is spin-cast onto a silicon substrate, forming a quasi-hexagonal array of nanostructures. The substrate is then annealed using microwaves to form an ordered array of horizontal cylinders. In the case of PS-*b*-P2VP, the BCP is then loaded with metal ions in an acidic solution, followed by oxygen plasma to reduce the metal ions and remove the polymer. (d) Microwave anneal reactor: the anneal takes place inside a sealed reaction tube, while the substrate is held above the solvent level using a custom-made glass support.

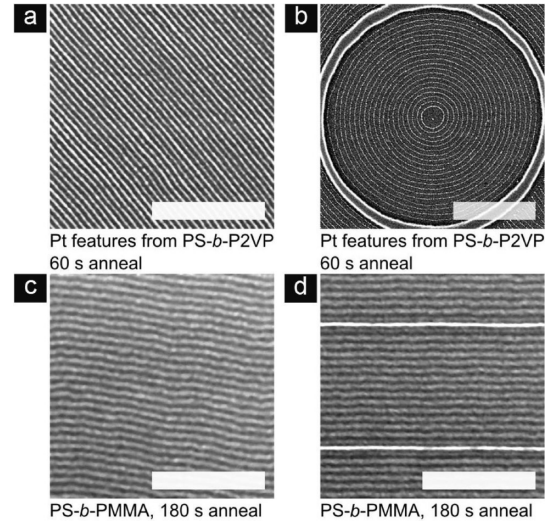

Figure 2. Examples of nanopatterns organized by microwave annealing. (a,b) SEM images of Pt lines templated from PS-*b*-P2VP (23.6k-10.4k) BCPs that were microwave annealed for 60 s at 130 °C in the presence of THF solvent. In (a), the substrate was unpatterned, and in (b), the substrate was flat Si(100) with a circular SiO_2 topological feature. (c,d) SEM images of PS-*b*-PMMA (45k-20k) BCPs that were microwave annealed for 180 s at 180 °C in the presence of THF solvent on (c) unpatterned Si(100) and (d) flat Si(100) with two parallel lines of SiO_2. All patterns were formed on 0.002−0.005 Ω · cm, Si(100), n-type wafers, and the scale bar in each picture represents 500 nm.

to bring about, in many cases, dramatic rate increases has become well-known in liquid phase reactions,[23] with some examples in the solid state, as well.[24−27] The effects of a range of microwave processing conditions on the quality and assembly speed of the annealed patterns are described, and the compatibility of the approach with directed assembly is demonstrated by performing a number of successful anneals in the presence of prefabricated topographical features (graphoepitaxy) intended to guide the ensuing BCP organization.

RESULTS AND DISCUSSION

Block Copolymers and the Microwave Anneal Apparatus. Block copolymers (polymers incorporating two or more chemically distinct repeat units, with each type grouped together into a "block") are schematically depicted in Figure 1a. We employ diblock copolymers containing two repeat units, A and B, which are subject to phase separation under appropriate conditions. With a covalent linkage between the two blocks, however, complete separation is not possible, and instead, ordered nanostructures (*e.g.*, spheres, cylinders, gyroid structures, and lamellae) are formed.[4,28−43] For this demonstration, poly(styrene)-*block*-poly(2-vinylpyridine) (PS-*b*-P2VP) or poly(styrene)-*block*-poly(methyl methacrylate) (PS-*b*-PMMA) (molecular structures are shown in Figure 1b) are used. For clarity, we also restrict ourselves to the subset of these polymers that form cylinders of either P2VP or PMMA surrounded by a PS matrix at equilibrium, although the approach should be general.

Figure 1c illustrates the basic experimental strategy used to prepare and visualize ordered BCP films on silicon surfaces. The BCPs were first spin-cast from solution to form thin films roughly 40 nm thick (determined by ellipsometry), and in all cases, the BCP film initially formed a quasi-ordered hexagonal pattern (see Figure S1 in Supporting Information). In order to increase the organization rate, these samples were then annealed in a conventional microwave reactor. As shown in Figure 1d, a solvent was always present in the reaction vessel, and the BCP-coated silicon substrates were placed on a microwave-safe glass support extending out of the solvent-filled volume. The reaction vessel was then sealed and irradiated with microwave energy. To investigate and optimize process conditions, various parameters were modulated including the microwave power, target temperature, irradiation time, BCP structure and molecular weight, solvent environment, and substrate resistivity. In cases where PS-*b*-P2VP block copolymers were employed, a metallization process was also undertaken to allow for pattern visualization by scanning electron microscopy (SEM). Metallization and BCP removal were carried out as described previously (and in the Methods section).[22,28]

SEM images of microwave annealed BCP films on silicon surfaces are shown in Figure 2. Panels a and b of Figure 2 correspond to nanostructures assembled from a PS-*b*-P2VP polymer with block molecular weights of

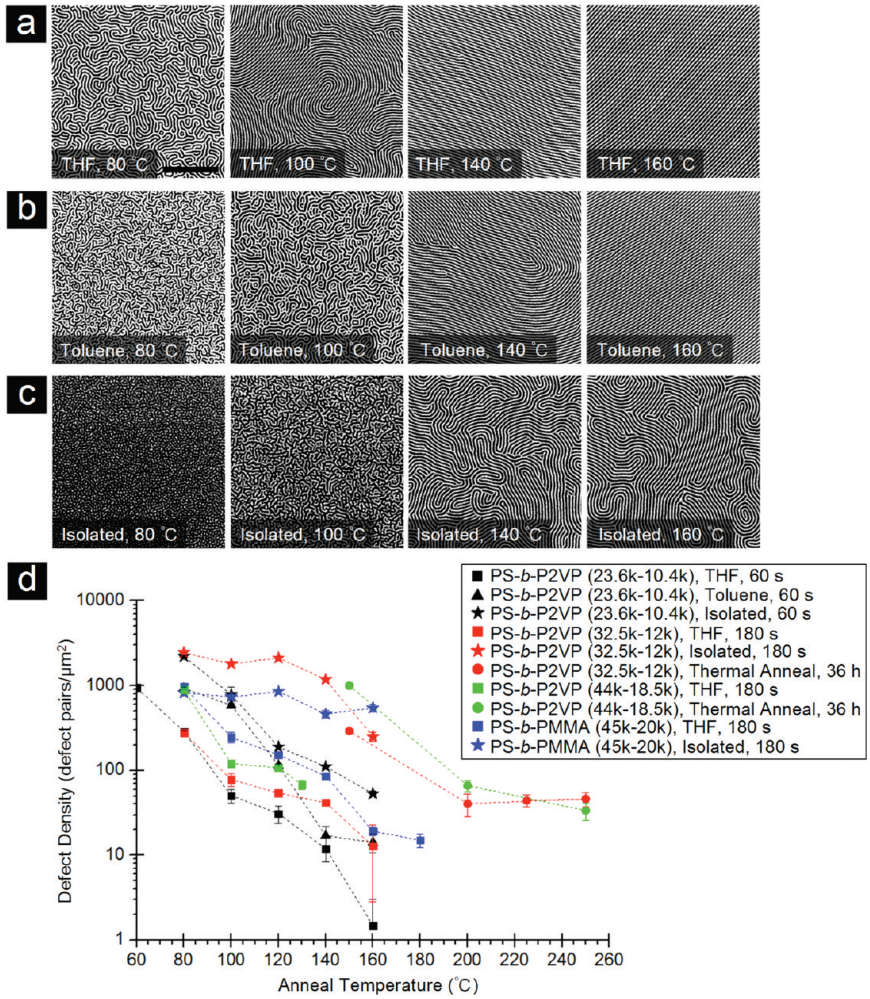

Figure 3. Solvent and temperature-based variations. (a−c) SEM images of Pt nanostructures templated from PS-*b*-P2VP (23.6k-10.4k) thin films that were microwave annealed at various temperatures (a) in the presence of THF, (b) in the presence of toluene, and (c) while isolated from solvents in a microwave reactor. In (a−c), the substrate was held at the target temperature for 60 s. (d) Plots of defect density *versus* anneal temperature for several BCPs, solvents, and anneal conditions. In all cases, the substrate was n-type (100) Si with resistivity in the range 0.002−0.005 Ω · cm. Dotted lines between data points are provided solely to facilitate discrimination between data sets. The scale bar corresponds to 500 nm.

23.6 kg/mol for the PS block and 10.4 kg/mol for the P2VP block. Henceforth, this and all BCPs will be denoted in the following format: PS-*b*-P2VP (23.6k-10.4k). These films were microwave annealed for 60 s each and then metallized (transformed into platinum nanostructures). BCP assembly in Figure 2a took place on the flat native oxide of Si(100), and horizontal lines with long-range order (~micrometers, Figure S2) were observed. Figure 2b shows an example of graphoepitaxy within a 1 μm diameter silica circle prepared *via* e-beam lithography, complete within 60 s. Figure 2c,d shows PS-*b*-PMMA (45k-20k) nanostructures prepared with 3 min microwave anneals on both a featureless Si(100) substrate (Figure 2c) and a flat Si(100) surface with parallel silica lines 500 nm apart, also synthesized through e-beam lithography (Figure 2d).

The BCP annealing steps for the samples in Figure 2 took place in the presence of tetrahydrofuran (THF) solvent, and sufficient microwave power was applied to achieve and hold the reaction vessel temperature noted in the images. The anneal hold time was fixed at 60 or 180 s, as indicated in the figure, while the temperature of the reaction vessel (as controlled by microwave intensity) was varied. It should be noted that the times reported represent the holding time at the selected anneal temperature. Prior to this time, a temperature ramp (15−60 s) is required to reach the target temperature, and afterward, another 30−90 s is required to air-cool the reaction tube. It is expected that some organization and assembly takes place during these periods. A video recording (running approximately 4 min in length) of one of the authors carrying out a full microwave anneal process is provided in the Supporting Information.

Microwave Annealing as a Solvothermal System. Various factors influence the assembly speed and defect density attainable through microwave-assisted annealing, and in Figure 3, the contributions of the anneal temperature

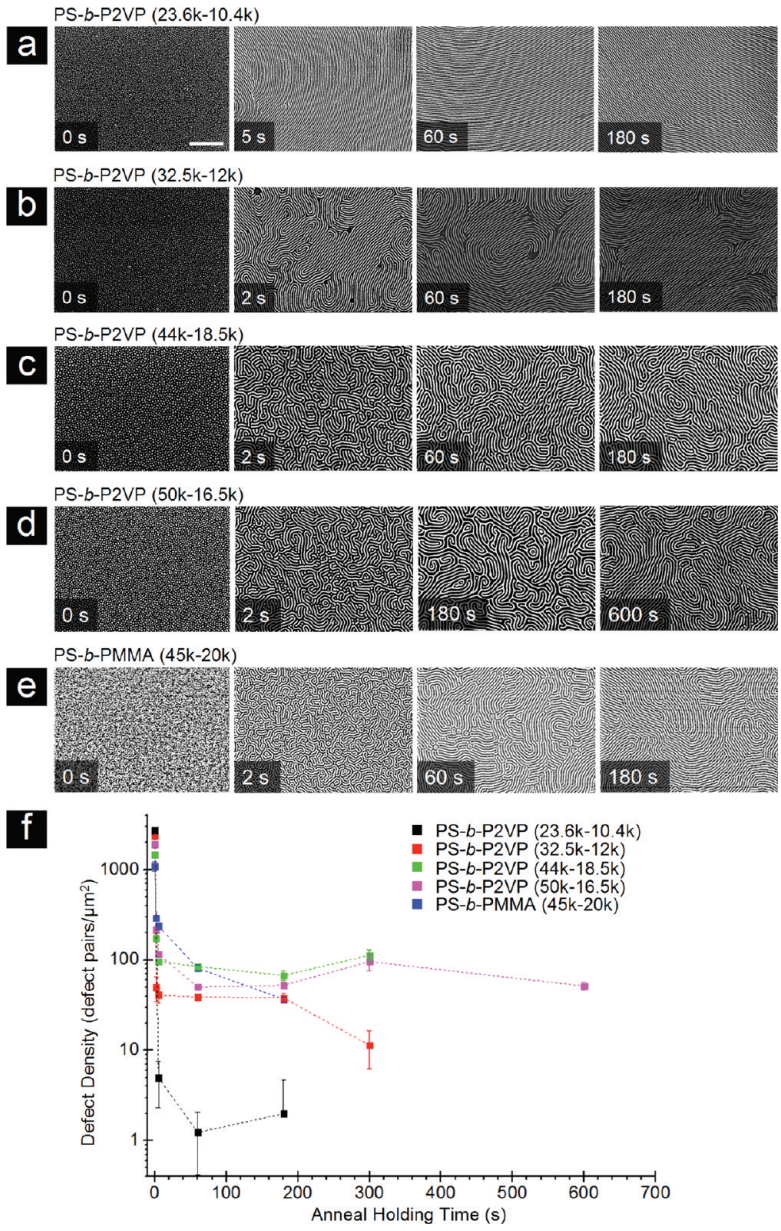

Figure 4. Influence of anneal time over the BCP organization. (a−d) SEM images of Pt nanostructures templated from PS-*b*-P2VP. (e) SEM images of block copolymer PS-*b*-PMMA (45k-20k). The first panel in each series shows the sample prior to annealing, and for each subsequent panel, the BCP thin films were microwave annealed at 130 °C in the presence of THF for various times ranging from 2 to 600 s. The scale bar corresponds to 500 nm for all images, and in each case, the substrates were 0.002−0.005 Ω · cm n-type Si(100). (f) Plots of the evolution of defect density for various BCPs microwave annealed in the presence of THF at 130 °C. Dotted lines between data points are provided solely to facilitate discrimination between data sets and are not intended to convey any interpolated information. SEM images of PS-*b*-PMMA were filtered to provide contrast enhancement and clarity. This was done by subtracting the background and then applying median and variance filters to reduce noise and increase the contrast between PS and PMMA structures. The original images are provided in the Supporting Information (Figure S14).

and solvent choice to the process are explored. In Figure 3a, conversion from a low-order, as-cast structure into a well-ordered cylindrical pattern is demonstrated for the PS-*b*-P2VP (23.6k-10.4k) BCP. For this experiment, the n-type Si(100) substrate had resistivities in the range of 0.002−0.005 Ω · cm, THF (widely used for solvent annealing) was present in the reaction vessel, and the chosen anneal temperature was held for 60 s. It is clear that, with increasing temperature, the order of the pattern after 60 s improves. Rudimentary fingerprint patterns are already apparent at 60 °C, while the domain size expands from less than 100 nm to several micrometers as the temperature is increased from 80 to 160 °C (see Supporting Figures S3 and S4). In order to investigate the effect of solvent, THF was replaced with toluene, and a similar trend was observed (Figure 3b): higher annealing temperatures lead to lower defect densities and larger domain sizes for a given period of time (60 s in this case). It is obvious in comparing Figure 3a,b that the composition of the solvent environment is important and that THF is the superior solvent: For example, nearly parallel lines persist across the entire 1.5 μm × 1.5 μm image at 140 °C with THF, but 160 °C is required with toluene to achieve a roughly comparable pattern. Thus, in a THF environment, lower microwave power is required to achieve a given degree of order. A series of PS-*b*-P2VP (23.6k-10.4k) thin films (see Figure S5) were subjected to similar anneal conditions as applied to those in Figure 3a, utilizing different solvents. The control experiment, presented in Figure 3c, demonstrates that less ordered patterns were attained when a BCP film was annealed in the absence of solvent. Other solvents investigated include water, ethanol, *N*,*N*-dimethylformamide, and *o*-dichlorobenzene, and they were found to be inferior to the commonly employed solvents, THF and toluene[4,37,44,45] (see Supporting Figures S6 and S7).

Using the image processing approach described in the Methods, the relationship between the anneal temperature and the density of defects—pairs of positive (*i.e.*, terminal points or dots) and negative (*i.e.*, junctions) disclinations—in the striped pattern are plotted for a range of PS-*b*-P2VP and PS-*b*-PMMA polymers,[29] as shown in Figure 3d. Several observations can be made: First, larger polymers require longer ordering times, and therefore, the organization of these polymers after 60 s tends to lag that of their smaller counterparts. Second, samples microwave annealed without an effective attendant solvent tend to be substantially more disordered. Finally, a comparison of microwave annealed BCP films with those annealed under conventional thermal conditions shows that far greater anneal times (36 h *vs* several minutes) and higher temperatures are required to achieve order in a conventional system than with a microwave-driven sol-

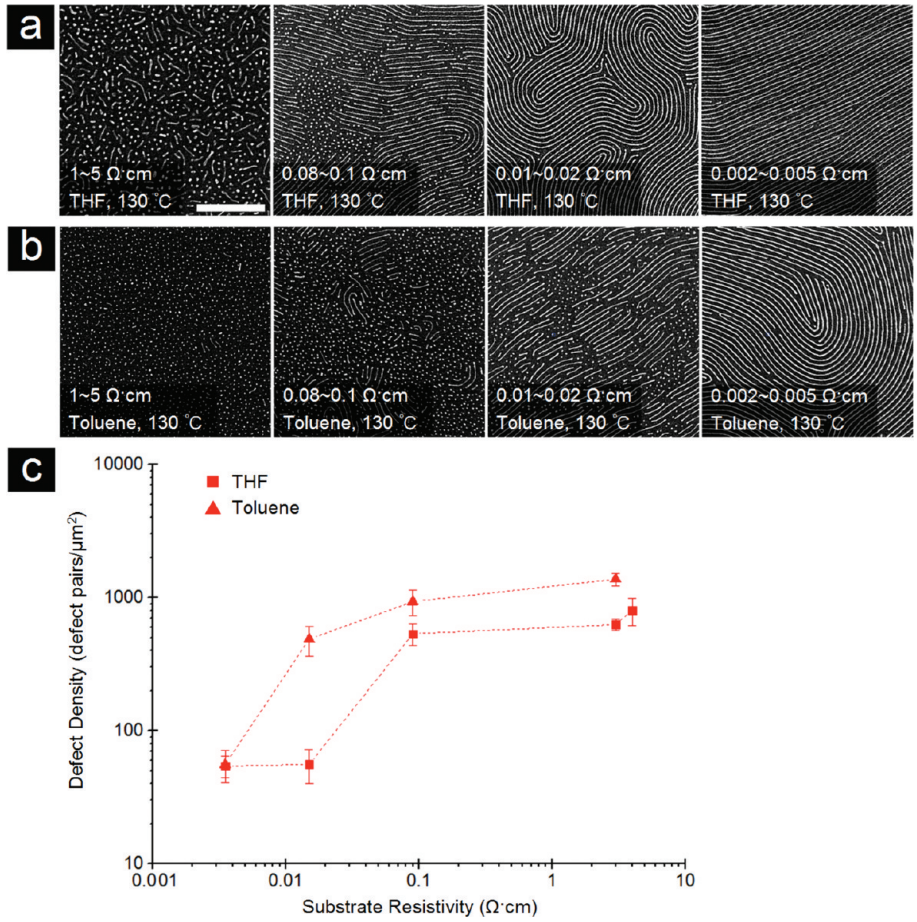

Figure 5. Resistivity-based variations in BCP organization. (a,b) SEM images of Pt nanostructures templated from PS-*b*-P2VP (32.5k-12.0k) thin films that were microwave annealed on Si(100) substrates of varying resistivity in the presence of (a) THF and (b) toluene. In both cases, the microwave anneal target temperature was 130 °C and the temperature was held for 180 s. The scale bar corresponds to 500 nm. (c) Plots of the evolution of defect density as the substrate resistivity is varied. Dotted lines between data points are provided solely to facilitate discrimination between data sets and are not intended to convey any interpolated information.

vothermal approach. SEM images of BCPs annealed under these conditions are provided in the Supporting Information (Figures S8 and S9).

To better understand the time evolution of BCP ordering during a microwave anneal, a series of experiments at constant anneal temperature was performed, and the results are presented in Figure 4. Several BCPs were irradiated for various lengths of time with sufficient microwave power to maintain a temperature of 130 °C in the presence of THF. The results for PS-*b*-P2VP (23.6k-10.4k) show that, after only 5 s at 130 °C, the measured defect density was reduced nearly 3 orders of magnitude, and after 180 s at 130 °C, an array of nearly parallel cylinders was attained over areas of approximately 10 μm^2 (Figure S2). A similar progression from disorder to order was observed for the PS-*b*-PMMA (45k-20k) BCP (Figure S10c), although the defect density was higher than that observed for PS-*b*-P2VP (23.6k-10.4k). The higher defect density is most likely the result of the slower reorganization kinetics of larger polymers, as the time required increases with increasing polymer size[4] (Figure 4). A considerably reduced defect density is observed after a relatively short anneal, even on the order of ~5 s, although the minimum defect density tends to be greater for larger polymers.

Influence of Substrate Resistivity. To investigate the role of substrate resistivity in the microwave-assisted solvothermal anneal process, BCP samples were spin-cast and microwave annealed on silicon substrates with various resistivities. Four n-type Si(100) substrates were investigated, with resistivities spanning 4 orders of magnitude: 1−5, 0.08−0.1, 0.01−0.02, and 0.002−0.005 Ω · cm. PS-*b*-P2VP (32.5k-12.0k) was used, and anneal experiments were conducted in the presence of both THF and toluene. The anneal target temperature was fixed at 130 °C, and the temperature was held for 180 s. In Figure 5, the organization of the BCP films was clearly observed to improve as the resistivity of the substrates was reduced. In the presence of THF, for instance (Figure 5a), a quasi-hexagonal pattern that differs little from completely unannealed BCP films was seen on the 1−5 Ω · cm substrates, while ordered cylinders were obtained on the 0.002−0.005 Ω · cm substrates. Similar results were observed in the toluene system. Defect

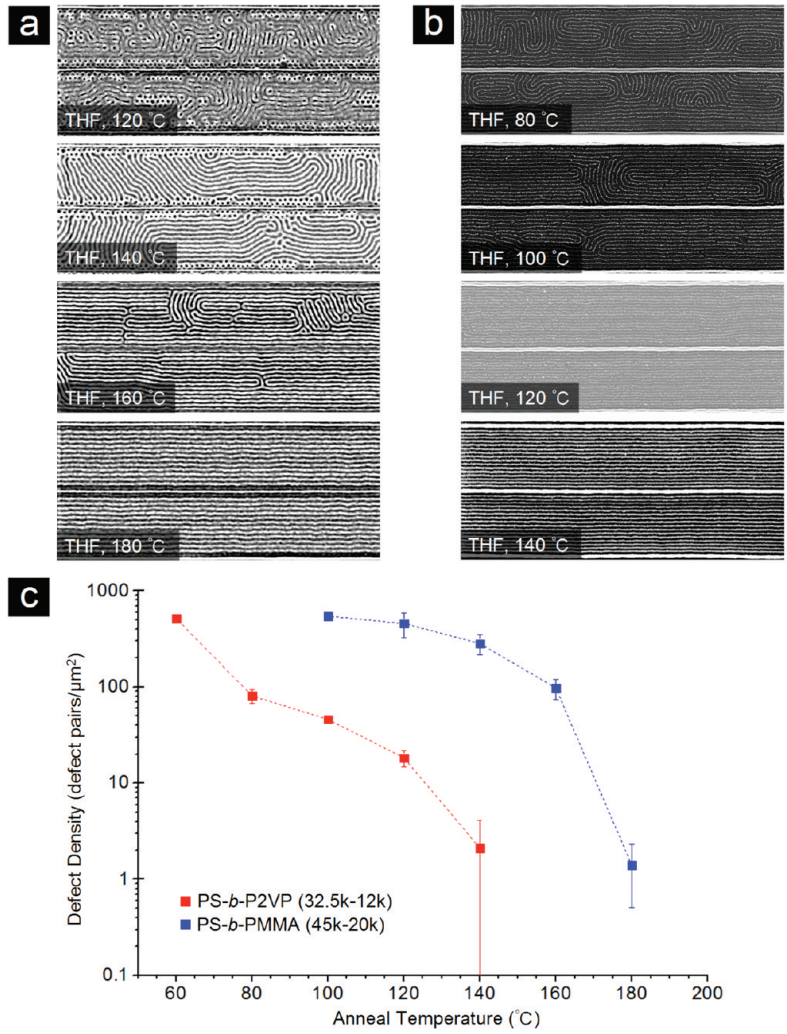

Figure 6. High-speed ordering of BCPs along graphoexpitaxial features. (a) SEM images of microwave annealed PS-*b*-PMMA (45k-20k) structures aligned along SiO_2 walls predefined by electron-beam lithography. In each panel, the BCP sample was held at the noted target temperature for 180 s in the presence of THF. (b) SEM images of Pt nanostructures templated from microwave annealed PS-*b*-P2VP (32.5k-12.0k) BCPs. In each panel, the BCP sample was held at the noted target temperature for 60 s in the presence of THF. The scale bars in all SEM images correspond to 500 nm. (c) Plots of the evolution of defect density as anneal temperature was varied. In all cases, the substrates were n-type Si (100) with resistivity in the range of 0.002−0.005 Ω · cm, and the solvent was THF. Images of PS-*b*-PMMA were enhanced in the same manner as those in Figure 4; original images are provided in the Supporting Information (Figure S15).

densities for these substrates were also quantified, and the results are plotted in Figure 5c. Free carriers in doped silicon are excited by the oscillating electric field of microwave radiation, and these excitations ultimately convert microwave energy into thermal energy within the silicon substrate. Lower resistivity (*i.e.*, high free carrier concentration) wafers appear to absorb microwave radiation more efficiently in our frequency range,[46] leading to greater substrate temperatures and faster BCP reorganization. These results suggest that doping-based control over the shape of BCP nanostructures could be exploited to achieve a controlled pattern of dots and lines through selective and patterned substrate doping.

The resistivity experiments suggest an annealing mechanism in which both a solvent-enriched environment and elevated substrate temperature play a role. Greater temperatures, which are rapidly induced in these microwave-assisted anneals, add thermal energy to the system, driving the system above T_g (the glass transition temperature) to facilitate a thermodynamically driven reorganization. Cooperatively, solvents infiltrating the BCP film, particularly at the increased pressure in the sealed reactor, would tend to plasticize the network, further encouraging reorganization. To experimentally compare microwave heating with thermal heating, the sealed microwave reaction vessels were loaded with a solvent and BCP-coated Si substrates and immersed in heated oil baths. A range of experimental conditions were screened, including oil bath temperatures from 80 to ~140 °C, but in all cases, it was observed that uneven heat distribution within the reaction tube led to solvent condensation on the

silicon substrate and removal of the BCP (see Figure S11).

Compatibility with Directed Self-Assembly. Intense efforts are being made to control the orientation and positioning of phase-separated BCP domains. Different strategies such as chemical prepatterning,[16,47−49] graphoepitaxy,[16,37,44,50] electric field alignment,[51−54] shear alignment,[55,56] and temperature gradients[57] have all been used to manipulate the assembly of BCP thin films over long ranges. The compatibility of microwave annealing with graphoepitaxy is demonstrated here: two-dimensional, wall-like structures of SiO_2 that act as topographical features were created using electron-beam lithography. In Figure 6a, the alignment of PS-*b*-PMMA (45k-20k) along parallel SiO_2 lines separated by 500 nm is demonstrated for a holding time of 180 s. The alignment and defect density of the microwave annealed structures improves as the anneal temperature is increased for this 3 min anneal. This effect is also apparent in the Pt structures formed from PS-*b*-P2VP, shown in Figure 6b. In both cases, the defect density decreased when topographical features were present, and the anneal temperature required to achieve this minimum order was reduced. In the case of PS-*b*-P2VP (32.5k-12k), the minimum defect density decreased from 15 defects/μm^2 on an unpatterned surface to 2 defects/μm^2 with graphoepitaxy, even with a lower temperature. The combined graphoepitaxy/microwave annealing was also capable of orienting BCPs in other patterns, and several examples are shown in Supporting Figures S12−S14.

CONCLUSIONS

Utilizing a commercial microwave reactor and common solvents, we have demonstrated a fast BCP annealing method compatible with ordered self-assembly on both flat and topographically patterned silicon surfaces. Through modification of the solvent environment, substrate resistivity, and target temperature, conditions that result in low defect densities on time scales significantly shorter than with conventional anneal techniques were pinpointed. This new microwave-mediated approach was demonstrated for the PS-*b*-P2VP and PS-*b*-PMMA polymer families, and it is reasonable to expect extensions to other self-assembling materials. Further research into substrates and BCPs will ultimately determine the generality, but given the short anneal times required, the microwave-mediated technique has the potential to nanopattern silicon interfaces for a range of commercial applications.

METHODS

Wafer Cleaning Procedure. Prime-grade 100 mm Si(100) wafers were cut into approximately 9 mm × 9 mm pieces. These silicon pieces were degreased in an ultrasonic bath of methanol, rinsed in acetone and ethanol, and then dried by a stream of nitrogen gas. Standard RCA procedures were then performed on the silicon. First, the silicon wafers were immersed in a hot solution of 30% NH_4OH (aq), 30% H_2O_2 (aq), and Millipore water in a ratio of 1:1:5 at 85 °C for 20 min. The wafers were then rinsed with water and immersed in another hot solution of 38% HCl, 30% H_2O_2, and Millipore water in a ratio of 1:1:5 at 85 °C for 20 min. The wafers were then rinsed with water and dried under a nitrogen gas flow. No additional surface treatments were employed.

Formation of Graphoepitaxial Features. Wall-like features were formed using electron-beam lithography. First, the silicon substrates were cleaned in piranha [3:1 mixture of concentrated H_2SO_4 and 30% H_2O_2(aq)] for 15 min, rinsed in water, and dried. The silicon squares were then baked at 150 °C for 15 min in air to remove water from the surface. A 1% solution of hydrogen silsesquioxane (HSQ) in methyl isobutyl ketone solvent was then spin-cast onto each substrate in a two-speed process: first, a spread cycle at 1000 rpm for 10 s, followed by a final spin at 3000 rpm for 30 s. Samples were then baked at 100 °C for 15 min in air, and subsequently loaded into a RAITH 150-TWO e-beam lithography system, which was used for all pattern writing. Following completion of pattern writing, the substrates were immersed in a 25% aqueous solution of tetramethylammonium hydroxide for 30 s, which removes all unexposed HSQ, leaving only wall-like SiO_2 features behind.

Generation of an Organized Array of Parallel Platinum Nanowires. The selected diblock copolymer was weighed and dissolved in toluene at room temperature by stirring overnight to make a ~1% w/w solution of polymer micelles. A 16 μL volume of the block copolymer solution was then spin-cast at 4200 rpm for 50 s over the selected silicon substrate and under an argon environment to form a thin film. The film thickness was verified by ellipsometry.

A Biotage Initiator 2.5 system that provides high-powered, focused microwave heating was used as a microwave anneal power source. The polymer-coated silicon substrates were first

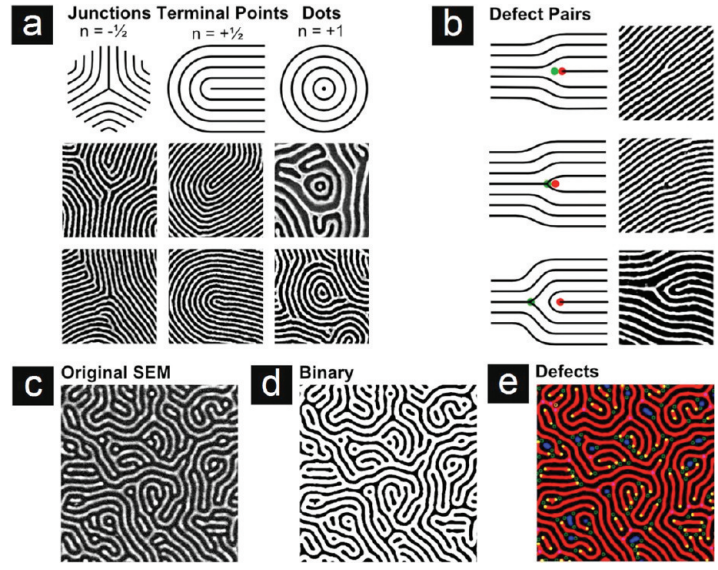

Figure 7. Automated defect analysis routine. (a) Component structures for all defects observed in the experiments with examples in both phases and associated disclination strengths. (b) Examples of defect pairs and the treatment of dislocations (top two) as pairs of positive (red) and negative (green) dislocations. (c) SEM image of metallic nanostructures on the surface of silicon prior to image analysis. (d) Appearance of the same SEM image following smoothing, noise reduction, and thresholding to facilitate identification of particles. (e) Image after defect types are identified and recorded (metal wires, red; dots, blue; junctions, magenta; terminal points, yellow; junctions in PS phase, green; terminal points in PS phase, orange).

cut into 4.5 mm × 9 mm shards in order to fit inside the Biotage-compatible reaction vessels. Inside, a microwave-safe glass support was used to hold the silicon shard flat above a small volume of the selected solvent (most commonly toluene or THF). The tube was then sealed, placed inside the reaction chamber, and irradiated with 2.45 GHz microwave energy. The Biotage feedback-controlled microwave power profile was used to reach the target temperature as rapidly and safely as possible. The system increases microwave power incrementally, then through temperature feedback control, it reduces the power to equilibrate at the preselected target temperature. This process requires roughly 15−90 s, depending on the target temperature and the microwave absorptivity of the solvent. Once the target temperature is reached, the preset anneal time begins. During the process, the input power was recorded, and the temperature of the glass reaction vessel was monitored using a built-in infrared sensor. Pressure inside the reaction vessel was also recorded and found to vary strongly with temperature and solvent. Pressures as high as 8 bar were observed. Dewetting of the BCP film was not observed in any of the experiments.

For microwave annealed PS-*b*-P2VP patterns, a metallization process was also performed. The annealed substrates were immersed in a solution of Na_2PtCl_4 (20 mM, aq) with HCl (1.6%, aq) for 3 h in a glass beaker. The samples were then rinsed thoroughly with water and dried in a stream of nitrogen gas. The ion-loaded BCP films were then reduced to platinum metal using an oxygen plasma (Harrick Plasma Cleaner/Sterilizer PDC-32G) at 0.12 Torr for 1 min.

Automated Defect Quantification. Measuring the defect density provides a quantitative means of describing order in BCP thin films,[29] so to minimize subjectivity and human error in the pattern analysis, we developed an automated image analysis tool dedicated to defect quantification. In our experiments, as-cast BCP thin films initially formed quasi-hexagonal arrays that were transformed into aligned cylindrical structures during solvent-assisted microwave annealing. In striped patterns, defects occur as pairs of positive and negative disclinations—which include dots, terminal points, and junctions—and these can occur in either of the BCP phases, or after metallization, in either the Pt metal or the interstices. The three defect components (dots, termini, and junctions) form the basis of all defects observed during solvent-assisted microwave annealing; examples of these component structures for the metalized PS-*b*-P2VP system are shown in Figure 7a. For the purposes of this paper, we treat dislocations as disclination pairs[58] (Figure 7b), combining the component defects to determine the total number of disclination pairs, as given by

$$N = \frac{2n_{\text{dots}} + n_{\text{termini}} + n_{\text{Y-junctions}} + 2n_{\text{X-junctions}}}{2}$$

The image analysis and defect counting were implemented using ImageJ.[59] First, the SEM image (Figure 7c) was digitally smoothed using nondirectional filters in order to reduce noise, and the background was subtracted; the image was then manually thresholded to define the particles of interest (Figure 7d); then, particles were analyzed and sorted by size and circularity to separate "dots" from "lines"; finally, connectivity of the "line" structures was analyzed to identify terminal and junction points; this is repeated with the interstitial phase to complete the process (Figure 7e).

Acknowledgment. This work was supported by the National Research Council of Canada, the University of Alberta, Alberta Innovates Technology Futures and the Natural Sciences and Engineering Research Council of Canada. The authors thank D. Hall, T. Elford, and B. Lazurko for access, training, and assistance on the microwave system, and D. Rider for useful discussions. D. Salamon is thanked for SEM support, and the University of Alberta NanoFab is acknowledged for e-beam lithography and clean room support.

Supporting Information Available: A video demonstrating a typical microwave anneal procedure, SEM images of various BCPs annealed under a range of conditions, photographs of equipment and samples, and differential scanning calorimetry traces. This material is available free of charge *via* the Internet at http://pubs.acs.org.

REFERENCES AND NOTES

1. Ito, T.; Okazaki, S. Pushing the Limits of Lithography. *Nature* **2000**, *406*, 1027–1031.
2. Harriott, L. Limits of Lithography. *Proc. IEEE* **2001**, *89*, 366–374.
3. Broers, A. N. Resolution Limits for Electron-Beam Lithography. *IBM J. Res. Dev.* **1988**, *32*, 502–513.
4. Bang, J.; Jeong, U.; Ryu, D. Y.; Russell, T. P.; Hawker, C. J. Block Copolymer Nanolithography: Translation of Molecular Level Control to Nanoscale Patterns. *Adv. Mater.* **2009**, *21*, 4769–4792.
5. Black, C. T.; Ruiz, R.; Breyta, G.; Cheng, J. Y.; Colburn, M. E.; Guarini, K. W.; Kim, H.; Zhang, Y. Polymer Self Assembly in Semiconductor Microelectronics. *IBM J. Res. Dev.* **2007**, *51*, 605–633.
6. Whitesides, G. M.; Grzybowski, B. Self-Assembly at All Scales. *Science* **2002**, *295*, 2418–2421.
7. Black, C. T.; Guarini, K. W.; Milkove, K. R.; Baker, S. M.; Russell, T. P.; Tuominen, M. T. Integration of Self-Assembled Diblock Copolymers for Semiconductor Capacitor Fabrication. *Appl. Phys. Lett.* **2001**, *79*, 409.
8. Stoykovich, M. P.; Nealey, P. F. Block Copolymers and Conventional Lithography. *Mater. Today* **2006**, *9*, 20–29.
9. Cheng, J. Y.; Ross, C.; Smith, H.; Thomas, E. Templated Self-Assembly of Block Copolymers: Top-Down Helps Bottom-Up. *Adv. Mater.* **2006**, *18*, 2505–2521.
10. Schwartz, E. L.; Bosworth, J. K.; Paik, M. Y.; Ober, C. K. In *Advances in Resist Materials and Processing Technology XXVII*; Allen, R. D., Ed.; SPIE: San Jose, CA, 2010; Vol. 7639, p 76390G-11.
11. Bates, F. S.; Fredrickson, G. H. Block Copolymers—Designer Soft Materials. *Phys. Today* **1999**, *52*, 32.
12. Park, M.; Harrison, C.; Chaikin, P. M.; Register, R. A.; Adamson, D. H. Block Copolymer Lithography: Periodic Arrays of $\sim 10^{11}$ Holes in 1 Square Centimeter. *Science* **1997**, *276*, 1401–1404.
13. *International Technology Roadmap for Semiconductors*, 2009 edition; Semiconductor Industry Association: San Jose, CA, 2009.
14. Park, S.; Lee, D. H.; Xu, J.; Kim, B.; Hong, S. W.; Jeong, U.; Xu, T.; Russell, T. P. Macroscopic 10-Terabit-per-Square-Inch Arrays from Block Copolymers with Lateral Order. *Science* **2009**, *323*, 1030–1033.
15. Stoykovich, M. P.; Muller, M.; Kim, S. O.; Solak, H. H.; Edwards, E. W.; de Pablo, J. J.; Nealey, P. F. Directed Assembly of Block Copolymer Blends into Nonregular Device-Oriented Structures. *Science* **2005**, *308*, 1442–1446.
16. Bita, I.; Yang, J. K. W.; Jung, Y. S.; Ross, C. A.; Thomas, E. L.; Berggren, K. K. Graphoepitaxy of Self-Assembled Block Copolymers on Two-Dimensional Periodic Patterned Templates. *Science* **2008**, *321*, 939–943.
17. Ruiz, R.; Kang, H.; Detcheverry, F. A.; Dobisz, E.; Kercher, D. S.; Albrecht, T. R.; de Pablo, J. J.; Nealey, P. F. Density Multiplication and Improved Lithography by Directed Block Copolymer Assembly. *Science* **2008**, *321*, 936–939.
18. Segalman, R. A. Materials Science: Directing Self-Assembly Toward Perfection. *Science* **2008**, *321*, 919–920.
19. Park, S.; Kim, B.; Xu, J.; Hofmann, T.; Ocko, B. M.; Russell, T. P. Lateral Ordering of Cylindrical Microdomains under Solvent Vapor. *Macromolecules* **2009**, *42*, 1278–1284.
20. *International Technology Roadmap for Semiconductors*, 2007 edition (Emerging Research Materials); Semiconductor Industry Association: San Jose, CA, 2007.
21. Welander, A. M.; Kang, H.; Stuen, K. O.; Solak, H. H.; Müller, M.; de Pablo, J. J.; Nealey, P. F. Rapid Directed Assembly of Block Copolymer Films at Elevated Temperatures. *Macromolecules* **2008**, *41*, 2759–2761.
22. Chai, J.; Wang, D.; Fan, X.; Buriak, J. M. Assembly of Aligned Linear Metallic Patterns on Silicon. *Nat. Nanotechnol.* **2007**, *2*, 500–506.

23. Kappe, C. O. Controlled Microwave Heating in Modern Organic Synthesis. *Angew. Chem., Int. Ed.* **2004**, *43*, 6250–6284.
24. Druzhinina, T.; Weltjens, W.; Hoeppener, S.; Schubert, U. S. The Selective Heating of Iron Nanoparticles in a Single-Mode Microwave for the Patterned Growths of Carbon Nanofibers and Nanotubes. *Adv. Funct. Mater.* **2009**, *19*, 1287–1292.
25. Petit, A.; Delmotte, M.; Loupy, A.; Chazalviel, J.; Ozanam, F.; Boukherroub, R. Microwave Effects on Chemical Functionalization of Hydrogen-Terminated Porous Silicon Nanostructures. *J. Phys. Chem. C* **2008**, *112*, 16622–16628.
26. Boukherroub, R.; Petit, A.; Loupy, A.; Chazalviel, J.; Ozanam, F. Microwave-Assisted Chemical Functionalization of Hydrogen-Terminated Porous Silicon Surfaces. *J. Phys. Chem. B* **2003**, *107*, 13459–13462.
27. Ko, C.; Lin, Y.; Chen, F. Microwave Annealing of Polymer Photovoltaic Devices. *Adv. Mater.* **2007**, *19*, 3520–3523.
28. Chai, J.; Buriak, J. M. Using Cylindrical Domains of Block Copolymers To Self-Assemble and Align Metallic Nanowires. *ACS Nano* **2008**, *2*, 489–501.
29. Harrison, C.; Adamson, D. H.; Cheng, Z.; Sebastian, J. M.; Sethuraman, S.; Huse, D. A.; Register, R. A.; Chaikin, P. M. Mechanisms of Ordering in Striped Patterns. *Science* **2000**, *290*, 1558–1560.
30. Jo, A.; Joo, W.; Jin, W.; Nam, H.; Kim, J. K. Ultrahigh-Density Phase-Change Data Storage without the Use of Heating. *Nat. Nanotechnol.* **2009**, *4*, 727–731.
31. Tang, C.; Lennon, E. M.; Fredrickson, G. H.; Kramer, E. J.; Hawker, C. J. Evolution of Block Copolymer Lithography to Highly Ordered Square Arrays. *Science* **2008**, *322*, 429–432.
32. Jenekhe, S. A.; Chen, X. L. Self-Assembly of Ordered Microporous Materials from Rod−Coil Block Copolymers. *Science* **1999**, *283*, 372–375.
33. Pochan, D. J.; Chen, Z.; Cui, H.; Hales, K.; Qi, K.; Wooley, K. L. Toroidal Triblock Copolymer Assemblies. *Science* **2004**, *306*, 94–97.
34. Warren, S. C.; Messina, L. C.; Slaughter, L. S.; Kamperman, M.; Zhou, Q.; Gruner, S. M.; DiSalvo, F. J.; Wiesner, U. Ordered Mesoporous Materials from Metal Nanoparticle-Block Copolymer Self-Assembly. *Science* **2008**, *320*, 1748–1752.
35. Mansky, P.; Liu, Y.; Huang, E.; Russell, T. P.; Hawker, C. Controlling Polymer−Surface Interactions with Random Copolymer Brushes. *Science* **1997**, *275*, 1458–1460.
36. Stoykovich, M. P.; Kang, H.; Daoulas, K. C.; Liu, G.; Liu, C.; de Pablo, J. J.; Müller, M.; Nealey, P. F. Directed Self-Assembly of Block Copolymers for Nanolithography: Fabrication of Isolated Features and Essential Integrated Circuit Geometries. *ACS Nano* **2007**, *1*, 168–175.
37. Bosworth, J. K.; Paik, M. Y.; Ruiz, R.; Schwartz, E. L.; Huang, J. Q.; Ko, A. W.; Smilgies, D.; Black, C. T.; Ober, C. K. Control of Self-Assembly of Lithographically Patternable Block Copolymer Films. *ACS Nano* **2008**, *2*, 1396–1402.
38. Park, C.; Cheng, J. Y.; Fasolka, M. J.; Mayes, A. M.; Ross, C. A.; Thomas, E. L.; De Rosa, C. Double Textured Cylindrical Block Copolymer Domains *via* Directional Solidification on a Topographically Patterned Substrate. *Appl. Phys. Lett.* **2001**, 79.
39. Bosworth, J. K.; Black, C. T.; Ober, C. K. Selective Area Control of Self-Assembled Pattern Architecture Using a Lithographically Patternable Block Copolymer. *ACS Nano* **2009**, *3*, 1761–1766.
40. Bai, J.; Zhong, X.; Jiang, S.; Huang, Y.; Duan, X. Graphene Nanomesh. *Nat. Nanotechnol.* **2010**, *5*, 190–194.
41. Lyuksyutov, S. F.; Vaia, R. A.; Paramonov, P. B.; Juhl, S.; Waterhouse, L.; Ralich, R. M.; Sigalov, G.; Sancaktar, E. Electrostatic Nanolithography in Polymers Using Atomic Force Microscopy. *Nat. Mater.* **2003**, *2*, 468–472.
42. Cheng, J. Y.; Mayes, A. M.; Ross, C. A. Nanostructure Engineering by Templated Self-Assembly of Block Copolymers. *Nat. Mater.* **2004**, *3*, 823–828.
43. Thurn-Albrecht, T.; Schotter, J.; Kastle, G. A.; Emley, N.; Shibauchi, T.; Krusin-Elbaum, L.; Guarini, K.; Black, C. T.; Tuominen, M. T.; Russell, T. P. Ultrahigh-Density Nanowire Arrays Grown in Self-Assembled Diblock Copolymer Templates. *Science* **2000**, *290*, 2126–2129.
44. Park, S.; Kim, B.; Yavuzcetin, O.; Tuominen, M. T.; Russell, T. P. Ordering of PS-*b*-P4VP on Patterned Silicon Surfaces. *ACS Nano* **2008**, *2*, 1363–1370.
45. Jung, Y. S.; Ross, C. A. Orientation-Controlled Self-Assembled Nanolithography Using a Polystyrene-Polydimethylsiloxane Block Copolymer. *Nano Lett.* **2007**, *7*, 2046–2050.
46. Sameshima, T.; Hayasaka, H.; Haba, T. Analysis of Microwave Absorption Caused by Free Carriers in Silicon. *Jpn. J. Appl. Phys.* **2009**, *48*, 021204.
47. Heier, J.; Genzer, J.; Kramer, E. J.; Bates, F. S.; Walheim, S.; Krausch, G. Transfer of a Chemical Substrate Pattern into an Island-Forming Diblock Copolymer Film. *J. Chem. Phys.* **1999**, *111*, 11101.
48. Ouk Kim, S.; Solak, H. H.; Stoykovich, M. P.; Ferrier, N. J.; de Pablo, J. J.; Nealey, P. F. Epitaxial Self-Assembly of Block Copolymers on Lithographically Defined Nanopatterned Substrates. *Nature* **2003**, *424*, 411–414.
49. Edwards, E. W.; Montague, M.; Solak, H.; Hawker, C.; Nealey, P. Precise Control over Molecular Dimensions of Block-Copolymer Domains Using the Interfacial Energy of Chemically Nanopatterned Substrates. *Adv. Mater.* **2004**, *16*, 1315–1319.
50. Segalman, R. A.; Yokoyama, H.; Kramer, E. J. Graphoepitaxy of Spherical Domain Block Copolymer Films. *Adv. Mater.* **2001**, *13*, 1152–1155.
51. Amundson, K.; Helfand, E.; Quan, X.; Hudson, S. D.; Smith, S. D. Alignment of Lamellar Block Copolymer Microstructure in an Electric Field. 2. Mechanisms of Alignment. *Macromolecules* **1994**, *27*, 6559–6570.
52. Xu, T.; Zhu, Y.; Gido, S. P.; Russell, T. P. Electric Field Alignment of Symmetric Diblock Copolymer Thin Films. *Macromolecules* **2004**, *37*, 2625–2629.
53. Boker, A.; Elbs, H.; Hansel, H.; Knoll, A.; Ludwigs, S.; Zettl, H.; Zvelindovsky, A. V.; Sevink, G. J. A.; Urban, V.; Abetz, V.; Müller, A. H. E.; Krausch, G. Electric Field Induced Alignment of Concentrated Block Copolymer Solutions. *Macromolecules* **2003**, *36*, 8078–8087.
54. Schmidt, K.; Schoberth, H. G.; Ruppel, M.; Zettl, H.; Hänsel, H.; Weiss, T. M.; Urban, V.; Krausch, G.; Böker, A. Reversible Tuning of a Block-Copolymer Nanostructure *via* Electric Fields. *Nat. Mater.* **2008**, *7*, 142–145.
55. Chen, Z.; Kornfield, J. A.; Smith, S. D.; Grothaus, J. T.; Satkowski, M. M. Pathways to Macroscale Order in Nanostructured Block Copolymers. *Science* **1997**, *277*, 1248–1253.
56. Hamley, I. W. The Effect of Shear on Ordered Block Copolymer Solutions. *Curr. Opin. Colloid Interface Sci.* **2000**, *5*, 341–349.
57. Bodycomb, J.; Funaki, Y.; Kimishima, K.; Hashimoto, T. Single-Grain Lamellar Microdomain from a Diblock Copolymer. *Macromolecules* **1999**, *32*, 2075–2077.
58. Kléman, M. *Points, Lines, and Walls: in Liquid Crystals, Magnetic Systems, and Various Ordered Media*; John Wiley: Chichester, NY, 1983.
59. Rasband, W. S. *ImageJ*; U.S. National Institutes of Health: Bethesda, Md, 1997.